Journal of Advanced Research in Natural and Applied Sciences
dergipark.org.tr/tr/pub/jarnas
Open Access

ISSN: 2757-5195 12 (3) (2026) 337-348 doi.org/10.28979/jarnas.1988347

Determination of Radial-Tangential Macroturbulence Stratification in the Solar Photosphere

İpek Hamami Çay[1], Mehmet Taşkın Çay[1]

Article Info
Received: 06 Jul 2026
Accepted: 29 Jul 2026
Published: 30 Sep 2026
Research Article

Abstract— This study models the depth-dependent behavior of Radial-Tangential (RT) macroturbulent velocity fields in the solar photosphere using high-resolution Fourier-domain analysis. The purpose of this investigation is to determine the velocity stratification to provide a useful empirical benchmark for evaluating both classical one-dimensional models and modern three-dimensional hydrodynamical simulations. The method employs 14 carefully selected, unblended iron lines from the solar flux atlas, which are analyzed through a disk-integration technique while fixing the solar synodic equatorial rotation and microturbulent velocity. Findings reveal that the macroturbulent velocity is not a constant value; it exhibits an overall decline from approximately 4.0 km s^{-1} in the deeper photospheric layers at an optical depth of $\log \bar{\tau} = -0.61$ to 3.0 km s^{-1} in the upper atmospheric layers at an optical depth of $\log \bar{\tau} = -1.47$. This velocity gradient is consistent with the convective deceleration of solar granulation as it rises through the atmosphere. The results show good quantitative agreement with prior wavelength-domain studies, supporting the interpretation that the detected stratification represents a physical property of the photosphere rather than a numerical artifact. These established profiles offer a useful semi-observational constraint for testing modern solar atmosphere simulations.

Keywords — *Solar photosphere, macroturbulence, depth dependence, Fourier analysis*

1. Introduction

Solar line profiles contain the fundamental imprint of unresolved photospheric velocity fields. In classical 1D spectroscopy, the empirical concept of macroturbulence was introduced to represent non-thermal motions occurring on scales larger than a photon mean free path, distinguishing it from smaller-scale microturbulent motions [1–3]. In this conventional framework, macroturbulence is not a directly observed physical entity but rather a phenomenological broadening parameter inferred from line-profile fitting, Fourier analysis, or inversion procedures when the underlying velocity field is not modeled explicitly [1, 4]. This distinction is important in the solar atmosphere; while granulation, organized convective upflows and downflows, and oscillatory motions represent actual physical phenomena, macroturbulence serves as the effective spectroscopic filter used to summarize their net contribution to the emergent line width and shape [2, 5].

Despite modern advances, solar-type stellar analyses still treat macroturbulence as a parameter of practical importance because non-thermal broadening, alongside stellar rotation, remains a primary

[1]ipek@istanbul.edu.tr (Corresponding Author); taskin@istanbul.edu.tr
[1]Department of Astronomy and Space Sciences, Faculty of Science, İstanbul University, İstanbul, Türkiye

determinant of line profiles, thereby directly influencing inferred stellar parameters and chemical abundances in 1D applications [5, 6]. The historical evolution of this field runs from the empirical detection of unresolved velocity fields to the formalization of macro- and microturbulent prescriptions, and ultimately to a renewed focus on depth dependence and model adequacy. Some of the earliest direct evidence that a depth-independent treatment of the solar atmosphere was inadequate came from Schmalberger's analysis of center-to-limb line profiles [7]. This early work demonstrated that matching observations required a stratified, depth-dependent radial non-thermal component that decreased rapidly with atmospheric height [7].

Subsequently, De Jager refined the physical interpretation by arguing that conventional micro- and macroturbulence should be treated as exact spectral filters applied to an underlying velocity spectrum rather than literal observables [8]. Applied to solar Fraunhofer lines, this framework suggested that most kinetic energy is confined to a narrow range of spatial scales corresponding to characteristic granular sizes, arguing against a fully developed, broad turbulence spectrum at the photospheric level [8]. A parallel and crucial methodological milestone was the utilization of Fourier techniques to disentangle rotational broadening from macroturbulent broadening. Smith demonstrated that rotation and macroturbulence leave distinctly different signatures in Fourier space, where rotation produces characteristic zeros and sidelobes, while macroturbulence acts primarily as a monotonic filter [9]. However, Smith also emphasized that separating these components becomes mathematically problematic when both velocities are small and comparable, requiring exceptionally high-quality data to overcome parameter degeneracy [9].

The Sun and solar-analogs lie precisely within this low-velocity regime ($v \sin i \approx 2$ km s^{-1}), where macroturbulent and rotational velocities are similar enough to generate substantial systematic uncertainties during direct spectrum fitting [5, 6]. Furthermore, Takeda noted that assigning a single macroturbulent value is not straightforward because it inherently depends on the formation depth, decreasing with atmospheric height [10]. In classical 1D model atmospheres, macroturbulence plays an indispensable structural role because these models cannot predict non-thermal line broadening from first principles, requiring free parameters to match observed profile shapes [2, 11]. This limitation directly impacts abundance determinations, as an inappropriate turbulent prescription can artificially map into systematic abundance trends with equivalent width [11].

This aforementioned rotational entanglement further exacerbates the uncertainties in 1D models; unless the rotational velocity is constrained via external techniques such as asteroseismology [6], recovering reliable macroturbulent dispersion via direct profile fitting is highly challenging [5]. While realistic 3D radiative-hydrodynamical simulations have reinterpreted macroturbulence by explicitly simulating inhomogeneous convective flows and reproducing line asymmetries without ad hoc parameters [2], 1D atmospheres remain widely used for large-scale stellar surveys and rapid parameter determinations [11–14]. Thus, evaluating the exact depth behavior of these empirical parameters within a 1D framework remains highly relevant.

Although analysis in Fourier domain provides a promising means of reducing the parameter degeneracy inherent in direct line profile fitting, its successful application requires spectra of exceptionally high quality. In particular, reliable Fourier diagnostics demand a carefully selected set of completely unblended spectral lines, as high-frequency noise and even weak blending can introduce distortions in the Fourier transform that mask the subtle signatures of macroturbulent broadening.

Despite decades of extensive research, a gap persists between empirical spectroscopy and physical interpretation. While historical studies by Schmalberger [7] and Kostik [15] inferred strongly stratified

macroturbulence components, classical solar analyses frequently adopt a single, depth-independent macroturbulent velocity for convenience. The geometric shape of the broadening kernel also remains a subject of ongoing discussion, with models ranging between simple Gaussian distributions and Radial-Tangential (RT) formulations [5, 12]. Although critics argue that the RT macroturbulence (RTM) may systematically yield velocity amplitudes roughly twice as large as those derived from isotropic Gaussian models, suggesting the latter as a more practical alternative for routine stellar applications [12], the RTM provides a geometrically motivated framework for unresolved stellar flux observations.

As demonstrated by Gray [4], the geometric projection of coupled radial and tangential flows accurately reproduces line profile shapes in the frequency domain, rather than treating macroturbulence as a purely phenomenological broadening parameter. Consequently, adopting the RTM framework is useful for separating these macroscopic velocity components without losing the physical imprint of convective stellar geometry. What remains insufficiently established is how the empirically inferred solar macroturbulent velocity varies with atmospheric depth when constrained by high-quality line-profile diagnostics in the Fourier domain and modeled via an RTM framework.

This study aims to fill this gap by conducting a high-resolution Fourier analysis on 14 carefully selected, blend-free Fe I lines from the Wallace et al. solar flux atlas [16]. By fixing the solar equatorial rotation velocity and applying a precise disk-integration technique, the depth stratification of the RT macroturbulent velocity ($\zeta_{\rm RT}$) across different optical depths ($\log \bar{\tau}$) is investigated. This focused investigation provides a useful empirical benchmark against which both classical 1D broadening prescriptions and realistic 3D hydrodynamical simulations can be rigorously evaluated. The remainder of this paper is organized as follows: Section 2 describes the observational materials and line selection criteria. Section 3 presents the mathematical formulation of the disk-integration procedure and application of Fourier transform. Section 4 discusses the main results and comparative literature analysis. Finally, Section 5 summarizes the conclusions of this work.

2. Materials and Preliminaries

The observational data analyzed in this study were obtained from the high-resolution Solar Flux Atlas compiled by Wallace et al. [16]. To ensure the statistical reliability and physical accuracy of the Fast Fourier Transform (FFT) analysis, the observational spectrum ideally should possess a resolving power (R) substantially greater than 100,000, as recommended by Gray [17]. The atlas was recorded using the Fourier Transform Spectrometer (FTS) at the McMath-Pierce Solar Telescope located at Kitt Peak National Observatory. It features an exceptional resolving power ranging from 350,000 to 700,000. This ultra-high resolution minimizes uncertainties in continuum placement and allows the wings of spectral lines to be traced reliably to the continuum level, while the minimal instrumental broadening of the FTS data makes the atlas an ideal baseline for evaluating subtle non-thermal velocity fields through profile diagnostics in the Fourier domain. Since the signature of RTM manifests as a distinct departure from pure Gaussian profiles in the line wings, the high resolution and high signal-to-noise ratio of this dataset provide an ideal foundation for a meticulous line profile analysis.

The theoretical line synthesis is carried out utilizing a one-dimensional, Local Thermodynamic Equilibrium (LTE) ATLAS9 [18] model atmosphere computed specifically for the Sun. The synthetic thermal profiles are generated via the SPECTRUM spectral synthesis program [19]. The required atomic parameters are retrieved from the Vienna Atomic Line Database (VALD) [20]. Experimentally determined oscillator strengths ($\log gf$) are preferentially selected to reduce systematic laboratory-scale

discrepancies. To construct a robust, unblended diagnostic framework, a systematic line-selection protocol was established based on the extensive iron line list of Takeda [21]. Whereas profile analyses in the wavelength domain can benefit from large datasets to improve statistical confidence, Fourier analyses require exceptionally high spectral purity for each individual line. Even weak blends or high-frequency noise can distort the Fourier transform and compromise the reliability of the derived line-profile diagnostics. Therefore, an initial wavelength filter was applied to focus primarily on the red region of the solar spectrum ($\lambda \gtrsim 6000$ Å), where the continuum is well defined and the local spectral line density is significantly lower, thereby substantially reducing the likelihood of significant blending in the line wings.

From this pre-filtered sample, the selection criteria were strategically tailored to isolate a final, high-purity set of 14 Fe I lines. First, following the weak-line suggestion of Gray [4], the core selection focused on lines with equivalent widths typically satisfying $EW < 55$ mÅ. This restriction ensures that the selected lines are within the linear regime of the curve of growth. As emphasized by Gray [4], maintaining a weak-line baseline ensures that the signature of macroturbulence on the main Fourier lobe can be reliably tracked to much higher frequencies without significant suppression by microturbulent sidelobes. By shifting the first zero points of the intrinsic thermal profile to higher spatial frequencies, these lines mitigate high-frequency noise contamination and significantly expand the usable Fourier domain. Crucially, to optimally capture the shallowest photospheric layers without introducing blending, our EW threshold was extended to include a single diagnostic line: Fe I λ5618 (59.8 mÅ). Despite its location slightly below the 6000 Å threshold and its marginally higher equivalent width, this specific line is entirely unblended compared to neighboring lines of similar strength. This spectral purity makes it an ideal diagnostic tool for probing the upper photospheric layers sampled in our depth-dependent velocity analysis while fully preserving the high-frequency tracking capability required in the Fourier domain.

Second, rather than selecting lines arbitrarily, the remaining candidates were systematically grouped according to their equivalent widths following the reference-set strategy of Sheminova [5]. This procedure provides a controlled and relatively uniform sampling of formation depths throughout the solar photosphere, spanning optical depths from $\log \bar{\tau} = -0.61$ to -1.47. All selected lines were further verified to have unblended wings extending smoothly to the continuum level. The atomic parameters retrieved from the VALD database, together with the equivalent widths and mean formation depths adopted from Takeda [21], for the selected 14 Fe I lines are summarized in Table 1.

Table 1. Atomic parameters, equivalent widths, mean formation depths, and derived RT macroturbulent velocities (ζ_{RT}) compared with Takeda (1995) for the selected 14 Fe I lines

λ(Å)	$\log gf$	$\log \gamma_{\rm Rad}$	$\log \gamma_{\rm Stark}$	$\log \gamma_{\rm VdW}$	EW (mÅ)	$\log \bar{\tau}$	ζ_{RT} [21] (km s^{-1})	ζ_{RT} (Present Work) (km s^{-1})
5618.614	−1.276	8.19	−5.45	−7.57	59.8	−1.18	3.53	3.38
6093.647	−1.500	8.33	−4.57	−7.51	34.3	−0.77	3.76	3.68
6151.623	−3.299	8.29	−6.16	−7.79	53.9	−1.41	3.13	3.37
6187.972	−1.720	7.75	−5.38	−7.54	55.0	−1.19	3.61	3.77
6226.748	−2.220	7.83	−5.27	−7.55	33.9	−0.84	3.78	4.08
6240.649	−3.233	6.88	−6.13	−7.79	52.8	−1.38	3.09	3.20
6498.943	−4.699	4.43	−6.21	−7.83	50.7	−1.47	3.05	3.12
6608.034	−4.030	8.30	−6.16	−7.79	20.8	−0.66	3.34	3.53
6627.527	−1.680	8.33	−5.33	−7.53	30.5	−0.74	4.00	3.78
6725.332	−2.300	8.40	−5.38	−7.54	20.8	−0.61	3.82	3.99
6726.640	−1.094	8.37	−4.66	−7.50	53.6	−1.08	3.68	3.61
7219.686	−1.690	8.23	−5.75	−7.74	54.0	−1.18	3.34	3.16
7461.531	−3.580	8.16	−6.11	−7.79	31.6	−0.90	3.33	4.00
7588.270	−2.060	8.84	−4.94	−7.51	35.5	−0.79	4.39	3.58

3. Methods

In the wavelength domain, the observed line profile represents a complex convolution of various broadening mechanisms, including thermal broadening, microturbulent velocity, macroturbulent velocity, and stellar rotation [17]. This intricate convolution inherently masks the individual signature of each distinct broadening mechanism, making direct decoupling mathematically challenging [9]. Conversely, within the Fourier frequency domain, this mathematical convolution converts into a straightforward scalar multiplication. This transformation provides a powerful diagnostic advantage, allowing each individual broadening mechanism to be isolated and rigorously investigated at distinct spatial frequency regions. For instance, the equivalent width determines the amplitude of the transform at the zero-frequency point, whereas the specific curvature and damping of the first sidelobe remain highly sensitive to the macroturbulent velocity profile. Thus, each non-thermal broadening mechanism can be examined solely through its distinct frequency-domain behavior, reducing the degeneracy present in wavelength space.

Technically and traditionally, the residual macroturbulent profile is extracted by dividing the Fourier transform of the observed line profile by the transform of a synthetic profile that incorporates all broadening mechanisms except macroturbulence. The isolated experimental profile is subsequently compared with theoretical macroturbulence models to derive the velocity dispersion. However, modern treatments demonstrate that the coupled effects of macroturbulence and rotation cannot be treated as a simple sequence of independent, isotropic convolutions. Macroturbulence possesses distinct radial and tangential components that convolve dynamically across the stellar surface depending on the local viewing geometry. To accurately model the combined effects of RTM and stellar rotation, this study employs the disk-integration technique proposed by Gray [4, 17].

A virtual solar surface is mapped onto a 501×501 spatial grid, yielding approximately 197,000 active coordinate points across the virtual solar disk. This spatial resolution was adopted to ensure adequate numerical sampling of the steep physical and geometric gradients encountered near the solar limb. At each specific coordinate (θ, ϕ), where θ represents the center-to-limb viewing angle and ϕ is the azimuthal angle, the macroscopic velocity field is modeled under the physical assumption of independent but equal radial and tangential components. The intrinsic local line profile at any given coordinate is computed using the following combined formulation:

$$\Theta(v,\theta,\phi) = \frac{1}{2}\left[\frac{1}{\sqrt{\pi}\zeta_R}\exp\left(-\left(\frac{v-v_{\rm rot}(\theta,\phi)}{\zeta_R}\right)^2\right) + \frac{1}{\sqrt{\pi}\zeta_T}\exp\left(-\left(\frac{v-v_{\rm rot}(\theta,\phi)}{\zeta_T}\right)^2\right)\right]$$

where $\zeta_R = \zeta_{RT}\cos\theta$ and $\zeta_T = \zeta_{RT}\sin\theta$ represent the local radial and tangential velocity dispersions. The term $v_{\rm rot}(\theta,\phi)$ denotes the local line-of-sight projection of the adopted solid-body synodic equatorial rotation velocity, while v denotes the Doppler velocity coordinate.

To construct the integrated total flux profile, each local coordinate profile $\Theta(v,\theta,\phi)$ is weighted by a linear limb-darkening law assuming a standard constant coefficient of $u = 0.6$, and then formally integrated over the entire visible solar disk. Finally, this integrated surface profile is combined with the theoretical thermal profile whose first zero amplitude is matched to the first zero amplitude of the observed profile in the Fourier domain. The Fast Fourier Transform calculations are executed utilizing Real Fast Fourier Transform (RFFT) algorithm implemented via the NumPy package [22].

Since the solar synodic equatorial rotation velocity is well established, it was fixed at $v_{\rm eq,syn} = 1.84$ km s^{-1} [17], thereby leaving the RT macroturbulent velocity dispersion (ζ_{RT}) as the sole free parameter to be optimized. Concurrently, the microturbulent velocity was fixed at $\xi_t = 0.5$ km s^{-1},

adopting the solar reference values from Gray [23] and Takeda [21]. Figure 1 illustrates an instant of the analysis.

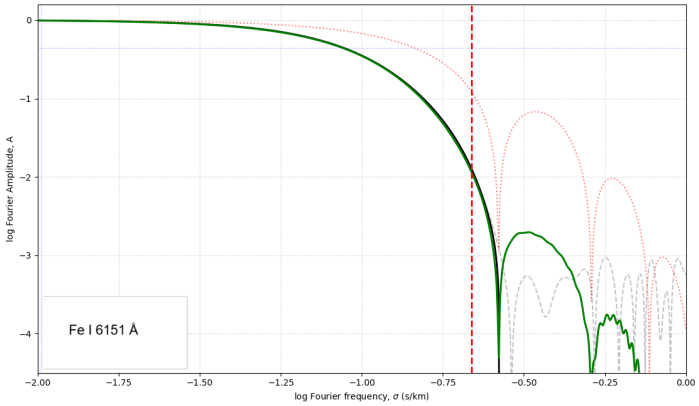


Figure 1. Application of FFT analysis to the Fe I 6151 Å line. The solid black line represents the Fourier transform of the observed profile, the dotted red line shows the Fourier transform of the pure thermal synthetic profile, and the solid green line indicates the Fourier transform of the synthetic profile after incorporating rotation and RT macroturbulence into the thermal profile. The amplitudes at the zero frequency (EW match) and the main lobe (macroturbulence effect) demonstrate close agreement. The dashed gray line denotes the noise level in the observed profile prior to the application of the Wiener filter (marked by the vertical dashed red line).

Stability tests show that variations in the microturbulent velocity (specifically testing $\xi_t = 0.0$ km s^{-1} and $\xi_t = 0.85$ km s^{-1}, a value commonly adopted for the Sun) do not introduce a substantial change in the profile curvature of the main Fourier lobe up to the mean noise level. This weak sensitivity is physically expected since weak absorption lines remain largely outside the saturated regime of the curve of growth where microturbulence dominates. Even for the strongest line in our sample, Fe I λ5618 (59.8 mÅ), which defines the upper limit of the sample's microturbulence sensitivity, the profile morphology within the main Fourier lobe ($\log\sigma \leq -1.2$) remains nearly unchanged over the tested range of ξ_t (see Figure 2)

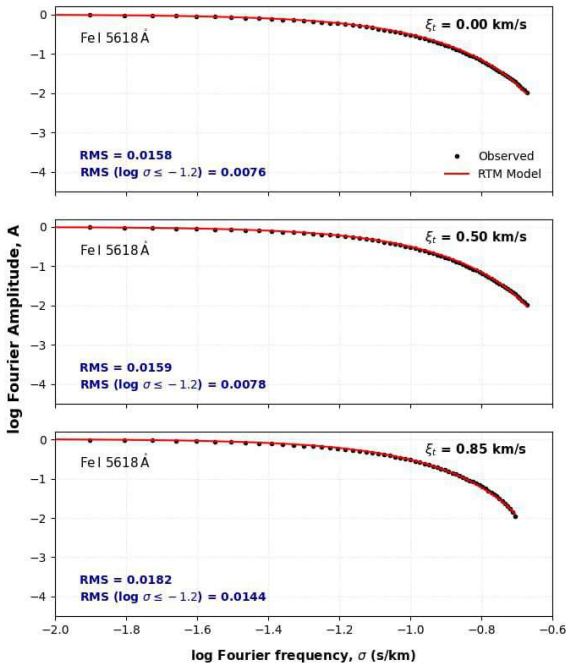


Figure 2. Microturbulence stability test for Fe I λ5618 Å line

These stability tests indicate that the low-frequency Fourier domain from which the macroturbulence solutions are derived is only weakly affected by parameter cross-talk. Because independently estimated pointwise uncertainties and a reliable covariance model for the processed Fourier-amplitude samples were not available, a conventional reduced chi-squared statistic could not be interpreted as a formal goodness-of-fit measure. The RMS deviation of the logarithmic Fourier-amplitude residuals was therefore used as an empirical objective function for determining the optimal ζ_{RT} value for each line. The RMS values reported in Figures 2 and 3 are calculated over the fitted Fourier interval; Figure 2 additionally reports the RMS calculated over the low-frequency region $\log\sigma \leq -1.2$ as a separate diagnostic of the profile agreement in that interval. For the 14 analyzed lines, the resulting RMS values range from 0.0140 to 0.0358 dex. Figure 3 presents the corresponding fits from which the $\zeta_{\rm RT}$ values listed in Table 1 were derived.

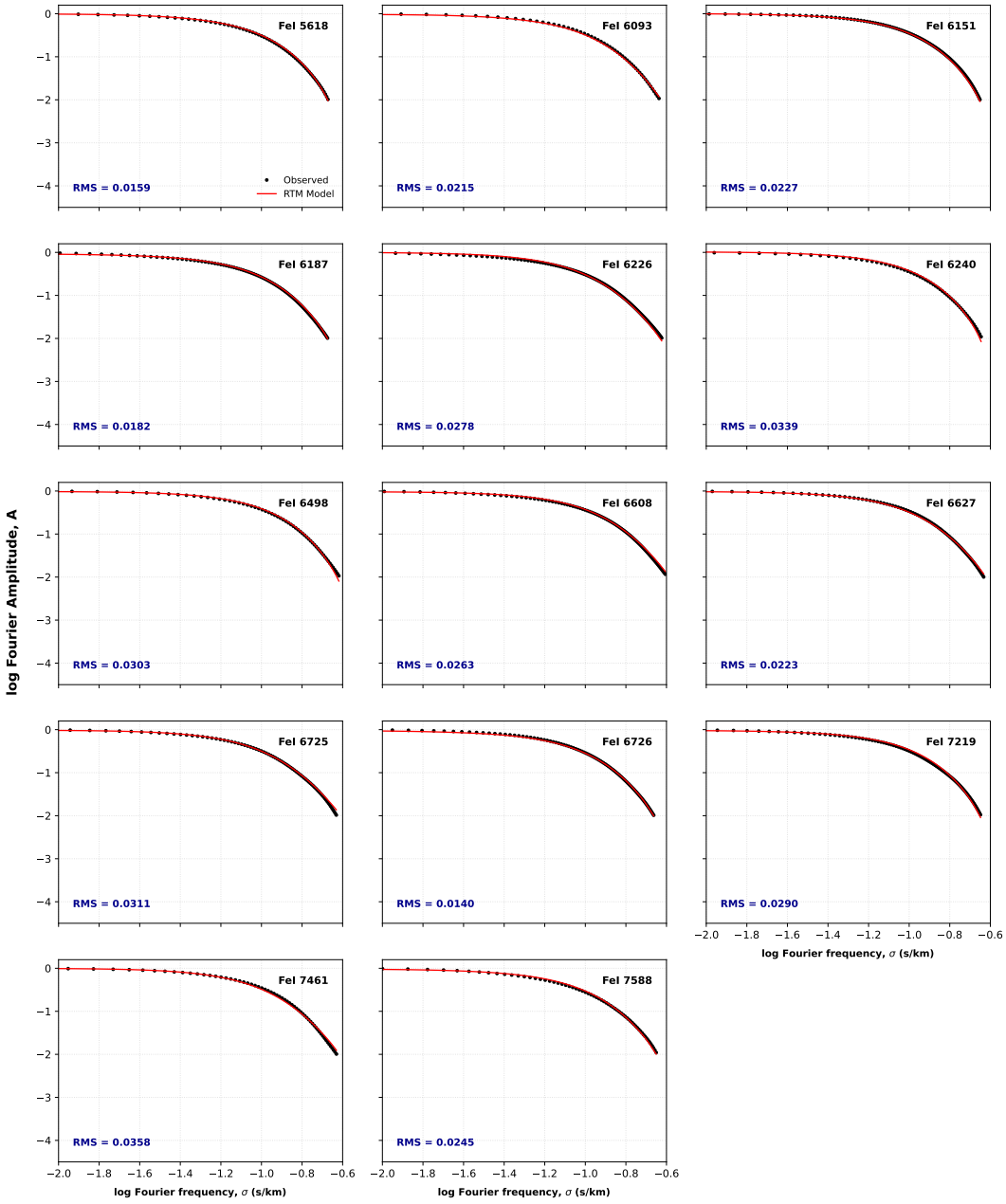


Figure 3. Final FFT comparisons between the observed and theoretical Fourier transforms for the complete set of lines

4. Results and Discussion

Although the solar spectrum contains hundreds of iron lines, the selection of the 14 specific Fe I lines analyzed in this study represents a deliberate compromise between spectral purity and depth coverage, based on the methodology derived from Gray [4] and Sheminova [5]. Takeda [21] originally utilized a much larger dataset of 275 Fe I lines for multi-parameter profile fitting in the wavelength domain. However, reliable isolation of the macroturbulent signature at high Fourier frequencies requires minimal blending, high spectral purity, and weak lines with $EW < 55$ mÅ. Accordingly, a subset of Fe I lines at wavelengths longer than approximately 6000 Å was extracted from Takeda [21]. The results of RTM velocity dispersion (ζ_{RT}) values for the analyzed spectral lines are presented in Table 1 together with mean optical depths of the lines.

Because the fitting statistic is based on the modulus of the Fourier transform within the low-frequency main lobe, weak convective line-profile asymmetries have a comparatively limited influence on the inferred broadening parameter. For a properly centered, nearly symmetric real line profile, the antisymmetric component associated with weak convective bisector distortions contributes to the imaginary part of the Fourier transform; its first-order signature therefore appears mainly in the phase, whereas its effect on the Fourier modulus is of higher order. Accordingly, the symmetric RTM kernel represents the even broadening component of the observed profile and does not explicitly model convective bisector asymmetries. At the level of the residuals obtained in the present fits, no systematic main-lobe mismatch attributable to these effects is apparent.

Our analysis reveals an overall increase in the macroturbulent velocity field with optical depth across the sampled solar photosphere. As the optical depth increases from the upper atmospheric layers ($\log \bar{\tau} = -1.47$) toward the deeper layers closer to the convection zone ($\log \bar{\tau} = -0.61$), the value of ζ_{RT} shows an overall increase from approximately 3.0 km s^{-1} to 4.0 km s^{-1}, yielding a total velocity gradient of $\Delta\zeta_{RT} \approx 1.0$ km s^{-1}. The dynamic behavior of the macroturbulent velocity dispersion as a function of optical depth is illustrated in Figure 4.

This inferred depth dependence indicates that treating macroturbulence as a single, depth-independent parameter throughout the solar atmosphere is an oversimplification. The inferred stratification is consistent with convective transport and granulation dynamics in the solar atmosphere. The deeper layers ($\log \bar{\tau} \sim -0.61$) are geometrically adjacent to the underlying, highly turbulent convection zone. In these deep regions, the kinetic energy dispersion driven by the vigorous upward flows of hot granules and the corresponding downward plunges of cooler, denser gas within intergranular lanes reaches its maximum intensity. However, as these convective plumes ascend into the shallower photospheric layers ($\log \bar{\tau} \sim -1.47$), they encounter a sharp decline in the atmospheric density gradient and experience overshoot buoyancy braking imposed by the subadiabatic, stable upper layers. This strong damping mechanism systematically slows down the convective plumes, directly reducing the fluctuation amplitude of the macroscopic velocity fields. Consequently, the steady decline in ζ_{RT} observed toward the upper photosphere is consistent with the vertical hydrodynamic deceleration of solar granulation.

Crucially, the quantitative velocity range and the upward depth-dependent trend determined in this study are in good agreement with the results obtained by Takeda [21], as clearly illustrated in Figure 4. Notably, both independent analysis results are tightly confined within a narrow velocity corridor between 3.0 and 4.0 km s^{-1}, and they share a similar non-linear curvature as they approach the deeper atmospheric layers. The close agreement between the present Fourier-domain analysis and the wavelength-domain profile fitting of Takeda [21], despite their different optimization procedures and evaluation criteria, supports the robustness of the inferred depth-dependent macroturbulent velocity

trend. In particular, the comparable velocity scales recovered for the same spectral lines indicate that the stratification is unlikely to be solely an artifact of the fitting domain or a particular numerical implementation. Although the two analyses are not independent of all underlying atmospheric and line-formation assumptions, their agreement strengthens the interpretation of the stratification as a genuine empirical property of solar photospheric line broadening.

The empirical $\zeta_{\rm RT}$ values should not be identified directly with the local RMS velocities of individual 3D hydrodynamical snapshots. A consistent mapping may instead be obtained by synthesizing the same disk-integrated Fe I profiles from ensembles of 3D snapshots and applying the identical Fourier-domain RTM analysis used here; the resulting line-dependent effective $\zeta_{\rm RT}$ values can then be associated with the contribution-function-weighted formation depths of the corresponding lines. Such a calibration would provide a practical link between physically resolved 3D velocity fields and the effective broadening parameters used in classical 1D stellar-survey analyses.

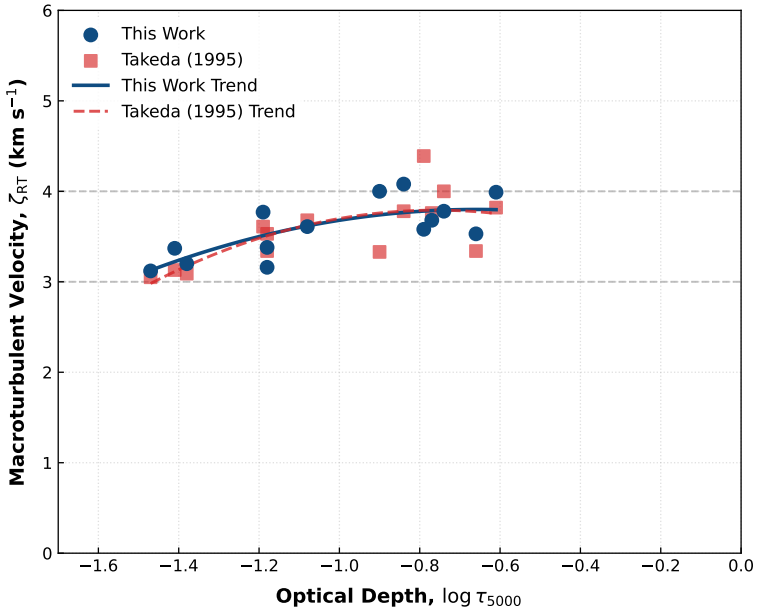


Figure 4. Derived depth dependence of RTM based on the analysis and comparison to Takeda [21]

Furthermore, the mean of the line-by-line values derived in the present analysis (3.59 km s^{-1}) agrees closely with the disk-integrated solar RTM value of 3.69 km s^{-1} obtained by Gray [4], indicating that the depth-dependent results remain consistent with the established mean solar RTM scale. The present analysis additionally provides information on the variation of this effective broadening parameter across the sampled line-formation depths. In contrast, while the Fourier-based analysis by Sheminova [5] also reported a general increase in velocity with atmospheric depth, the absolute velocity scale obtained in that study (1.9 to 2.6 km s^{-1}) is systematically lower than our results and the Takeda [21] benchmark. This discrepancy is largely associated with the choice of the broadening kernel; Sheminova [5] adopted an isotropic Gaussian Macroturbulence (GM) model, whereas the present study uses an RTM kernel. Takeda & UeNo [12] noted that the RTM framework may systematically yield velocity amplitudes roughly twice as large as those derived from isotropic Gaussian models, suggesting the GM as a simpler, more practical alternative for routine resolved disk applications. However, from a stellar physics perspective, the deliberate adoption of the RTM framework in this study is motivated by the following considerations.

First, the RTM physically incorporates the anisotropic nature of stellar granulation by explicitly splitting the macroscopic field into distinct radial (vertical convective upflows/downflows) and tangential

(horizontal overshoot flows) geometric components, whereas the GM assumes an isotropic spatial distribution. Second, for unresolved stellar flux observations, which constitute the primary data source in stellar astrophysics, the RTM has been shown to reproduce integrated line profiles and constrain equatorial rotation velocities ($v \sin i$) to within approximately 4% under the tested conditions [4]. While critiques favor the GM for resolved disk profiles, the finest observational constraints for comprehensive stellar analysis originate from unresolved flux spectra. Third, our weak-line strategy in the Fourier domain reduces the cross-talk between rotation and macro-velocity fields. Finally, although the RTM remains an empirical broadening prescription within a 1D framework, its explicit radial–tangential geometry provides a physically motivated description of unresolved convective line broadening in disk-integrated stellar spectra. Therefore, the higher velocity scale obtained via the RTM framework should not be regarded simply as an overestimation relative to Gaussian-macroturbulence values; rather, it reflects the distinct geometric definition and projection properties of the adopted anisotropic kernel.

5. Conclusions

In this study, the depth-dependent behavior of RTM velocity fields, a critical non-thermal broadening mechanism in the solar photosphere, has been comprehensively modeled utilizing a high-resolution disk-integration technique in the Fourier frequency domain. Our results show that the macroturbulent velocity dispersion (ζ_{RT}) is not constant but exhibits an overall decline from approximately 4.0 km s^{-1} in the deeper photospheric layers ($\log \bar{\tau} = -0.61$) to 3.0 km s^{-1} in the upper atmospheric layers ($\log \tau = -1.47$). The close agreement between the present Fourier-domain results and the wavelength-domain profile fitting of Takeda [21], despite the different optimization procedures and evaluation criteria employed, supports the robustness of the inferred depth-dependent macroturbulent velocity trend. The comparable velocity scales obtained for the same spectral lines indicate that the stratification is unlikely to be solely an artifact of the fitting domain or a particular numerical implementation. Although this agreement does not remove the atmospheric and line-formation assumptions shared by the analyses, it strengthens the interpretation of the stratification as a genuine empirical property of solar photospheric line broadening.

By combining a carefully selected set of 14 weak, blend-free Fe I lines with a 501×501 disk-integration grid, the present analysis recovers a depth-dependent RTM velocity scale that is higher than the values obtained with isotropic Gaussian prescriptions discussed above. This higher scale should not be regarded simply as a systematic overestimation; rather, it reflects the distinct geometric definition and projection properties of the anisotropic RT kernel, which provides a physically motivated, though still empirical, description of unresolved convective broadening within a 1D framework. Together with the close agreement with the wavelength-domain analysis of Takeda [21] and the RMS values ranging from 0.0140 to 0.0358 dex, the resulting depth-dependent ζ_{RT} profile provides a semi-observational benchmark for testing disk-integrated Fe I line profiles synthesized from modern 3D hydrodynamical solar-atmosphere simulations. A consistent comparison can be established by applying the same Fourier-domain RTM procedure to synthetic profiles generated from ensembles of 3D snapshots and deriving corresponding line-dependent effective ζ_{RT} values.

Finally, the Fourier-based disk-integration methodology presented in this work can be effectively extended to the atmospheric analysis of other late-type, slow-rotating dwarf stars. By reducing the parameter degeneracy between micro- and macroturbulence through analysis of the main Fourier lobes, this framework may support more consistent chemical abundance determinations and studies of stellar photospheric velocity fields.

Author Contributions

All authors equally contributed to this study. They have all read and approved the final version of the study.

Declaration

This study is not derived from any thesis or dissertation.

Conflicts of Interest

The authors declare no conflict of interest.

Ethical Review and Approval

No approval from the Board of Ethics is required.

Artificial Intelligence (AI) Use Statement

The authors declare that no artificial intelligence (AI) tools were used in the conception, design, or generation of the main/original results of this study, including data collection, analysis, or interpretation. AI tools were used only for editing assistance, such as improving language, readability, or reference formatting. The authors are solely responsible for the content, accuracy, and integrity of the work.

References

[1] C. Aerts, J. Puls, M. Godart, M.-A. Dupret, *Collective pulsational velocity broadening due to gravity modes as a physical explanation for macroturbulence in hot massive stars*, Astronomy & Astrophysics 508 (1) (2009) 409–419. [link]

[2] M. Asplund, Å. Nordlund, R. Trampedach, C. Allende Prieto, R. F. Stein, *Line formation in solar granulation. I. Fe line shapes, shifts and asymmetries*, Astronomy & Astrophysics 359 (2000) 729–742. [link]

[3] N. Serebriakova, A. Tkachenko, C. Aerts, *The ESO UVES/FEROS Large Programs of TESS OB pulsators: II. The physical origin of macroturbulence*, Astronomy & Astrophysics 692 (2024) A245. [link]

[4] D. F. Gray, *A solar-flux line-broadening analysis*, The Astrophysical Journal 857 (2) (2018) 139. [link]

[5] V. A. Sheminova, *Turbulence and rotation in solar-type stars*, Kinematics and Physics of Celestial Bodies 35 (3) (2019) 129–142. [link]

[6] A. P. Doyle, G. R. Davies, B. Smalley, W. J. Chaplin, Y. Elsworth, *Determining stellar macroturbulence using asteroseismic rotational velocities from Kepler*, Monthly Notices of the Royal Astronomical Society 444 (4) (2014) 3592–3602. [link]

[7] D. C. Schmalberger, *Depth dependence of turbulence in the solar photosphere*, The Astronomical Journal 67 (1962) 586. [link]

[8] C. De Jager, *Micro- and macroturbulent motions and the velocity spectrum of the solar photosphere*, Solar Physics 25 (1) (1972) 71–80. [link]

[9] M. A. Smith, *Applications of Fourier analysis to broadening of stellar line profiles. IV. A technique for separating macroturbulence from rotation in solar-type stars*, The Astrophysical Journal 208 (1976) 487–499. [link]

[10] Y. Takeda, S. Honda, S. Kawanomoto, H. Ando, T. Sakurai, *Behavior of Li abundances in solar-analog stars. II. Evidence of the connection with rotation and stellar activity*, Astronomy & Astrophysics 515 (2010) A93. [link]

[11] R. Collet, M. Asplund, R. Trampedach, *Three-dimensional hydrodynamical simulations of surface convection in red giant stars. Impact on spectral line formation and abundance analysis*, Astronomy & Astrophysics 469 (2) (2007) 687–706. [link]

[12] Y. Takeda, S. UeNo, *Does the radial-tangential macroturbulence model adequately describe the spectral line broadening of solar-type stars?*, Publications of the Astronomical Society of Japan 69 (3) (2017) 46. [link]

[13] Z. Magic, A. Weiss, M. Asplund, *The Stagger-grid: A grid of 3D stellar atmosphere models. III. The relation to mixing length convection theory*, Astronomy & Astrophysics 573 (2015) A89. [link]

[14] Z. Li, T. Li, Y. Zhou, S. Bi, *Validating the 1D-3D coupling stellar models via asteroseismology of 18 Kepler main-sequence stars*, The Astrophysical Journal 996 (1) (2026) 83. [link]

[15] R. I. Kostik, *Damping constant and turbulence in the solar atmosphere*, Solar Physics 78 (1) (1982) 39–57. [link]

[16] L. Wallace, K. H. Hinkle, W. C. Livingston, S. P. Davis, *An optical and near-infrared (2958–9250 Å) solar flux atlas*, The Astrophysical Journal Supplement Series 195 (1) (2011) 6. [link]

[17] D. F. Gray, The observation and analysis of stellar photospheres, Cambridge University Press, 2022. [link]

[18] R. Kurucz, ATLAS9 stellar atmosphere programs and 2 km/s grid, Robert Kurucz CD-ROM 13 (1993) Accessed 12 May 2026. [link]

[19] R. O. Gray, C. J. Corbally, *The calibration of MK spectral classes using spectral synthesis. I. The effective temperature calibration of dwarf stars*, The Astronomical Journal 107 (1994) 742–746. [link]

[20] N. E. Piskunov, F. Kupka, T. A. Ryabchikova, W. W. Weiss, C. S. Jeffery, *VALD: The Vienna Atomic Line Data Base*, Astronomy and Astrophysics Supplement Series 112 (1995) 525–535. [link]

[21] Y. Takeda, *Analyses of line profiles in the solar flux spectrum for determining rotation and micro/macro turbulence*, Publications of the Astronomical Society of Japan 47 (3) (1995) 337–354. [link]

[22] C. R. Harris, K. J. Millman, S. J. van der Walt, R. Gommers, P. Virtanen, D. Cournapeau, E. A. Wieser, J. Taylor, S. Berg, ..., T. E. Oliphant, *Array programming with NumPy*, Nature 585 (7825) (2020) 357–362. [link]

[23] D. F. Gray, *A test of the micro-macroturbulence model on the solar flux spectrum*, The Astrophysical Journal 218 (1977) 530–538. [link]